ChemBioChem

Combining Chemistry and Biology

Chemistry Europe

European Chemical Societies Publishing

Accepted Article

Title: Protection and isolation of bioorthogonal metal catalysts using monolayer-coated nanoparticle nanozymes

Authors: Xianzhi Zhang, Stefano Fedeli, Sanjana Gopalakrishnan, Rui Huang, Aarohi Gupta, David C. Luther, and Vincent Rotello

To be cited as: *ChemBioChem* 10.1002/cbic.202000207

Link to VoR: https://doi.org/10.1002/cbic.202000207

WILEY-VCH

10.1002/cbic.202000207

WILEY-VCH

COMMUNICATION

Protection and isolation of bioorthogonal metal catalysts using monolayer-coated nanoparticle nanozymes

Xianzhi Zhang, Stefano Fedeli, Sanjana Gopalakrishnan, Rui Huang, Aarohi Gupta, David C. Luther, and Vincent M. Rotello*

E-mail: rotello@chem.umass.edu
* Department of Chemistry
University of Massachusetts Amherst
710 North Pleasant Street, Amherst, Massachusetts 01003, United States

Supporting information for this article is given via a link at the end of the document.

Abstract: We present here demonstration of the protection of biorthogonal transition metal catalysts (TMCs) in biological environments using self-assembled monolayers on gold nanoparticles (AuNPs). Encapsulation of transition metal catalysts (TMCs) into this hydrophobic environment preserves catalytic activity in presence of pH conditions and complex biological media that deactivates free catalyst. Significantly, the protection afforded by these 'nanozymes' extends to isolation of the catalyst 'active site', as demonstrated by the independence of rate over a wide pH range, in strong contrast to the behavior of the free catalyst.

Introduction

Bioorthogonal chemistry provides a tool for performing reactions in biological system without interfering with natural processes.[1-3] Bioorthogonal processes can be used to generate imaging and therapeutic agents in biosystems with high specificity for reactants. Bioorthogonal *catalysis* is a particularly attractive strategy, providing access to enzyme-like systems.[4-7] Transition metal catalysts (TMCs) are excellent candidates for bioorthogonal processes, featuring high reactivity, selectivity and ready access to non-biological processes.[8,9] Researchers have developed ruthenium-[10-12] palladium-[9,13-19] and iron-[20] based catalysts for generation of fluorophores and therapeutics as well as for *in situ* protein modification. However, the direct use of TMCs is challenging due to poor water solubility, low stability and limited biocompatibility of these reactive systems.[21] In particular, these TMCs can be very sensitive to physiological pH variations, limiting their applicability in biological systems.[22]

Incorporating TMCs in nanomaterials can enhance both their solubility and stability in biological environments.[8,23,24] As an example, previous reports have demonstrated the ability to attach palladium catalyst on micron-size polystyrene scaffold for therapeutic drug activation [25], or into mesoporous silica nanoparticles for controlled catalysis. [26]

Recently, we have developed nano-sized reactors that show enzymatic kinetic behavior (i.e. nanozymes) by encapsulating TMCs into the self-assembled monolayers of 2 nm AuNPs.[23] Through appropriate design, these NZs are able to respond to exogenous stimuli such as supramolecular processes,[8,27] and localize at desired intracellular/extracellular,[28] and biofilm locations. [29]

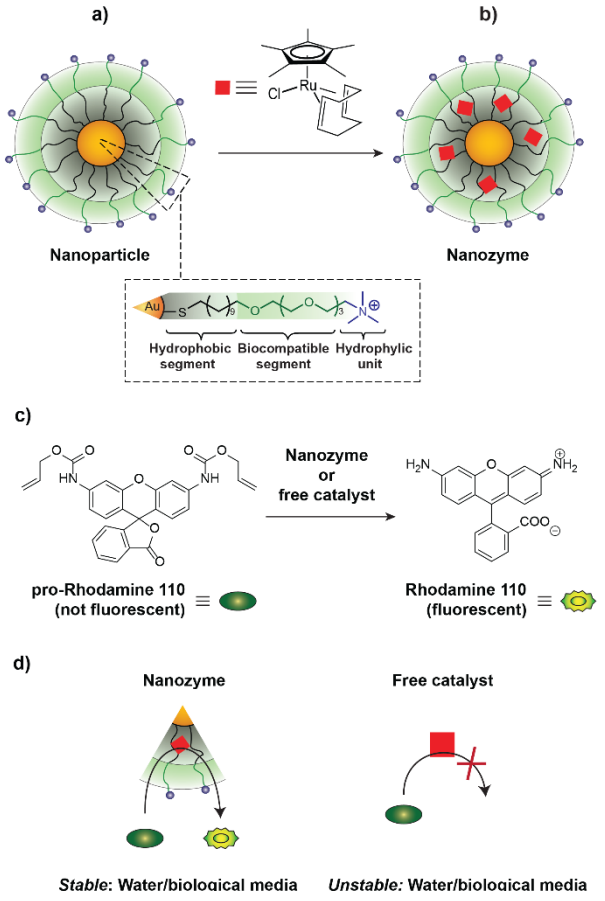

Figure 1. Schematic representation of the insulation properties of the nanozyme. (a) Structure of AuNP-TTMA containing the hydrophobic aliphatic chain (black), the hydrophobic segment (green) and the cationic head group (blue). (b) Structure of TMCs and encapsulation of TMCs within AuNP-TTMA. (c) Catalytic deprotection of non-fluorescent pro-Rho into fluorescent Rho though free TMCs or nanozymes. (d) Retention of catalytic activity in nanozyme in different environments due to supramolecular interactions with monolayer.

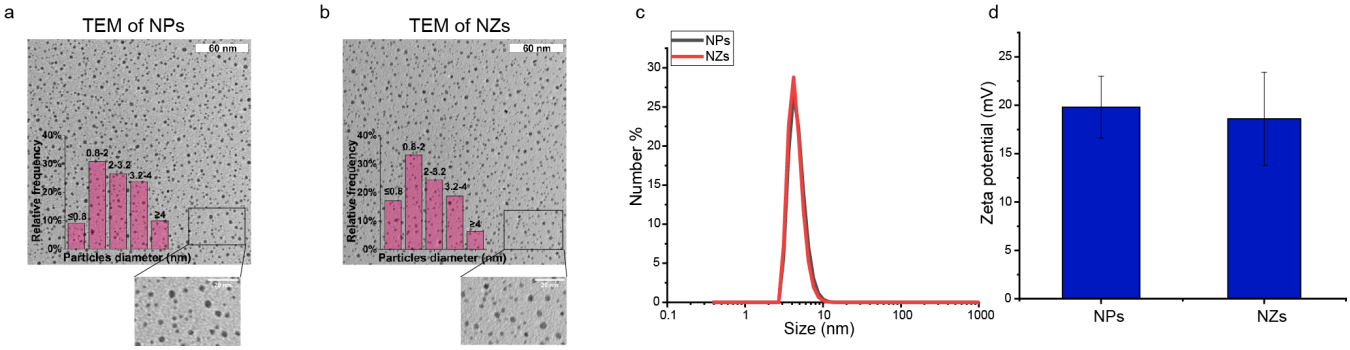

Figure 2. Characterization of AuNP-TTMA and NZ-TTMA. (a) and (b) TEM image of AuNP-TTMA (2.4±1.0 nm) and NZ-TTMA (1.8±1.1 nm) confirmed that no aggregation occur after encapsulation (c) The DLS result showed similar hydrodynamic diameter of AuNP-TTMA and NZ-TTMA (d) Zeta potential of AuNP-TTMA and NZ-TTMA indicated no significant change of surface charge. Each experiment had 3 replicates, and the error bars represent the standard deviation.

Here we demonstrate the ability of the particle monolayer to protect the TMCs, preserving activity in complex biological media as well as over the full range of physiological pH. Going well beyond protection of the TMCs activity, the monolayer isolates the catalyst from the outside environment, as demonstrated by minimal changes in catalyst efficiency with pH, in stark contrast to the free catalyst that showed strong pH dependence.

Result and discussion

AuNP (2 nm AuNP core) scaffolds (AuNP-TTMA) were designed with three structural features (shown in **Figure 1a**) – (1) a hydrophobic aliphatic monolayer (2) a hydrophilic tetra ethylene glycol spacer to enhance biocompatibility (3) a terminal quaternary ammonium to improve solubility in aqueous environment. The hydrophobic monolayer has been used previously to encapsulate hydrophobic drugs[30] as well as TMCs.[8] **Figure 1b** shows the TMCs utilized in this study Cp*Ru(cod)Cl [(Cp* = pentamethylcyclopentadienyl cod = 1,5-cyclooctadiene)].[10] This TMC is able to perform the uncaging of the allyoxycarbonyl group on substrates. The substrate utilized is the non-fluorescent pro-Rhodamine 110 (pro-Rho) (**Figure 1c**) which is converted into the fluorescent Rhodamine 110 (Rho) upon catalysis, providing straightforward determination of activity.

The nanozyme (NZ-TTMA) was synthesized from pentanethiol capped core AuNP-TTMA using a place exchange reaction.[23] Then the TMCs were encapsulated into the monolayer through nanoprecipitation followed by ultrafiltration to remove the unbound TMCs (details in experimental section). The diameter of the overall particle is ~7 nm in water with 2 nm core which is verified by DLS and TEM measurements respectively and is not affected by the encapsulation of the TMCs (**Figure 2,** experimental details in Supporting information). The TMCs loading was obtained by ICP-MS analysis, revealing ~20 TMCs molecule per nanoparticle (Table S1).

The ability of the AuNP-TTMA scaffold to protect the TMCs was evaluated first by measuring the catalytic activity in aqueous media (pH = 7.4). The catalytic activity was evaluated by measuring the increase in fluorescence intensity due to the activation of pro-Rho. (**Figure 1c**) and compared with free TMCs. Previous studies demonstrated that catalyst is retained in the monolayer,[27] so pro-dye activation occurred *in situ*. According to the calibration curve of Rhodamine 110 (**Figure S1**), the rate of activation was calculated in **Figure 3**. The results show a remarkable difference in the behavior of the two systems. It is seen in **Figure 3a** and **Figure 3b** that the free TMC is completely deactivated within 4 h of incubation. On the contrary, ~60% of the catalytic activity of the TMCs was retained even after 4 h with NZ-TTMA. Clearly, the AuNP-TTMA monolayer can stabilize the TMC over a prolonged duration in aqueous environments.

We next evaluated the stability of the NZ-TTMA in simulated biological environments. For this, the catalytic activity of the NZ-TTMA as well as the free TMCs were measured in 1% serum concentration. As can be seen in **Figure 4**, the catalytic activity of

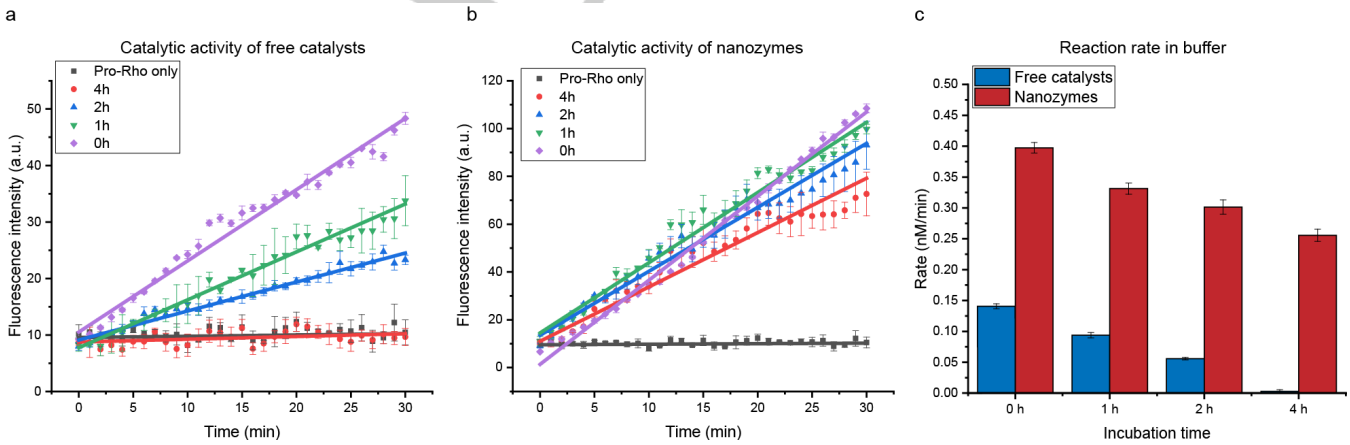

Figure 3. Stability of nanozyme in aqueous media. (a) Catalytic activity of free TMCs with time. For the free TMCs, catalytic activity drastically reduced within 4 h. (b) Catalytic activity of nanozyme with time. For nanozyme no significant change in activity was observed. (c) Comparison of rates of activation of TMC and nanozyme at 0,1,2 and 4h. Each experiment had 3 replicates, and the error bars represent the standard deviation.

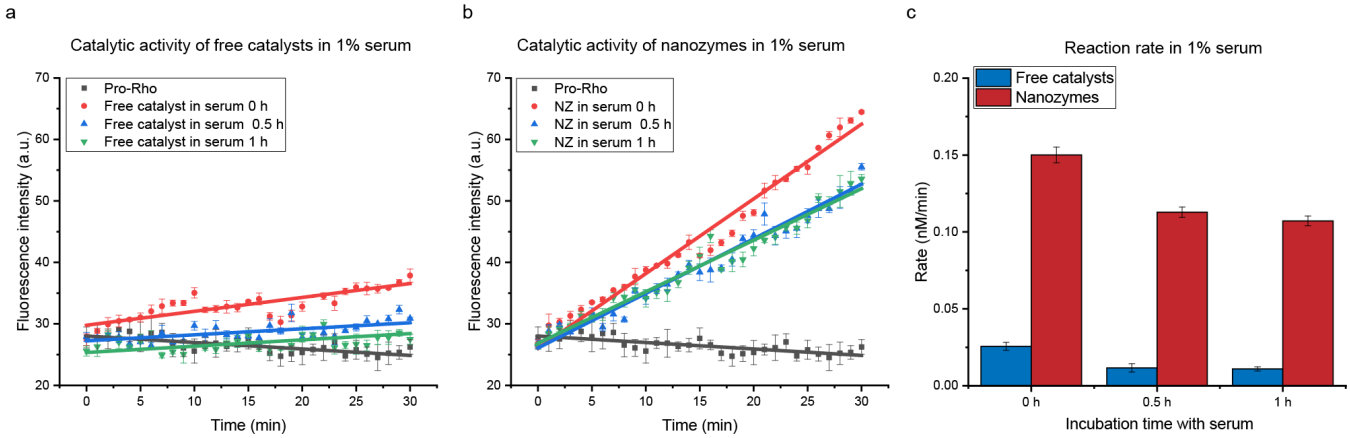

Figure 4. Stability of NZ-TTMA in serum. (a) Catalytic activity of free TMCs with time. The activity of the free TMCs was drastically reduced in serum. (b) Catalytic activity of NZ-TTMA with time. For nanozyme no significant change in activity is observed between 0.5 and 1h. (c) Comparison of rates of activation of TMCs and NZ-TTMA at 0, 0.5 and 1 h. Each experiment had 3 replicates, and the error bars represent the standard deviation.

the NZ-TTMA remains unchanged while the activity of the free TMCs drops significantly with over 30 min. The catalytic activity of the NZ-TTMA is slightly reduced with respect to aqueous media, attributed to the formation of a protein corona[31] around cationic nanoparticles that modestly decreases activity in NZ-TTMA featuring surfaces such as NZ-TTMA that resist irreversible protein binding.[32]

Having established protection of the catalyst, we next explored the ability of the monolayer to isolate the TMC from the external environment. To test for isolation, we measured catalytic activity at different pH. According to literature, the product Rhodamine is not sensitive to pH change.[33, 34] **Figure 5** shows a dramatic difference between the activity of the two systems at physiological and acidic pH. Free TMCs have excellent catalytic activity at pH = 4.1, but over 99% of the activity was lost at pH = 5.5 and 7.4. In contrast, the NZ-TTMA retained comparable activity over the range of pH 4.1-7.4. This result indicates that the AuNP monolayer is able to shield the encapsulated TMCs from the external environment, including acids. We hypothesize that the hydrophobic pocket generated by strong supramolecular interactions between the TMCs and the aliphatic monolayer is responsible for the insulating property of the AuNP scaffold.

Conclusion

In summary, we have demonstrated that the monolayer of AuNP-TTMA protects and isolates biorthogonal TMC catalysts - through supramolecular interactions. Encapsulation of catalyst into AuNP-TTMA hydrophobic pockets eliminates environmental effects, preserving high catalytic activity. This NZ-TTMA strategy provides highly promising strategy for the application of bioorthogonal catalysis in a wide range of fundamental, imaging, and diagnostic uses.

Experimental section

Encapsulation of ruthenium catalyst into AuNP-TTMA: 2.0 mg of ruthenium catalyst were dissolved in 1 mL of acetone and added dropwise to 1 mL of 15 μM of AuNP-TTMA. The resulting solution was stirred at room temperature for half an hour followed by slowly evaporating acetone by Rotavapor. Excess of TMC was removed by 0.22 μm PES membrane filter. Then the dispersion was washed with ultra-centrifugal filters (MWCO = 10 KDa), washing with Milli-Q water three more times after no color observed in the flow through. The concentration of NZ-TTMA was measured by the absorption at 506 nm and the TMC amount was measured by ICP-MS by tracking ^{101}Ru and ^{197}Au.

Synthesis of pro-Rhodamine: Rhodamine 110 (1 eq, 100mg) and pyridine (70μL, 3.2 eq) was dissolved in 2mL dimethylformamide (DMF) in ice bath. Allyl chloroformate (87 μL,

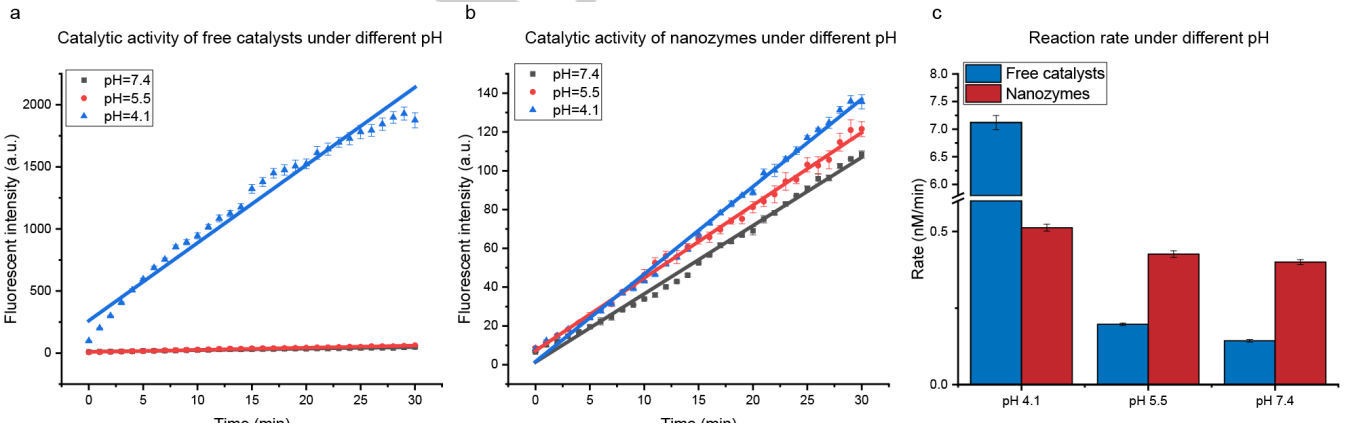

Figure 5. Stability of nanozyme in acidic and physiological pH. (a) Catalytic activity of free TMCs at pH = 4.1, 5.5 and 7.4. It was observed that activity drastically reduced within at pH = 5.5 as compared to pH = 4.1(b) Catalytic activity of nanozyme with time. No significant change in activity was observed (c) Comparison of rates of activation of TMCs and nanozymes at pH = 4.1, 5.5 and 7.4. Each experiment had 3 replicates, and the error bars represent the standard deviation.

3 eq) was added to the solution by dropwise. The resulting solution was stirred in ice bath for two hours and warmed up to room temperature overnight. The product was purified by a column with 2:1 hexane to ethyl acetate as eluent. Pro-Rhodamine 110 was obtained as a pinkish white powder. ^{1}H-NMR (400 MHz, DMSO-d6) 10.05 (s, 2H), 8.0 (d, 1H), 7.77 (t, 1H) 7.7 (t, 1H), 7.55 (s, 2H), 7.24 (d, 1H), 7.14 (d, 2H), 6.69 (d, 2H), 5.8 (m, 2H), 5.35 (d, 2H), 5.22 (d, 2H), 4.61 (d, 4H).

Protection from NZ-TTMA: NZ-TTMA and free TMC were incubated in PBS (pH = 7.4) for 4h, 2h, 1h and 0h or PBS containing 1% serum for 0h, 0.5h and 1h at room temperature prior kinetic study. After incubation, a solution containing 10 μM of pro-Rho and 200 nM NZ-TTMA or 4 μM free TMC was prepared in 96 well black plate. The kinetics study was done by detecting the increase of fluorescence of Rhodamine (λ_{ex} = 488 nm, λ_{em} = 521 nm) by Molecular Devices SpectraMax M2 microplate reader at 37 °C. Each experiment comprised three replicates

Kinetic study of insulation: 10 μL of pro-Rho in DMSO was added into 96 well black plate, followed by adding 100 μL of NZ-TTMA or free TMC solution in PBS buffer (pH = 7.4, 5.5 and 4.1), obtaining the final concentration of 10 μM of pro-Rho and 200 nM of NZ-TTMA or 4 μM free TMC. The kinetic study was based on tracking the increase of fluorescence intensity of Rhodamine (λ_{ex} = 488 nm, λ_{em} = 521 nm) by Molecular Devices SpectraMax M2 microplate reader at 37 °C. Each experiment comprised three replicates.

Acknowledgements

This research was supported by NIH EB022641

Keywords: Bioorthogonal catalysis • nanozymes • protection • insulation • monolayer

WILEY-VCH

COMMUNICATION

Entry for the Table of Contents

We demonstrate the retained catalytic activity of bioorthogonal transition metal catalysts through encapsulation within the hydrophobic monolayer of gold nanoparticles. This encapsulation strategy stabilizes the catalyst in environmental conditions like serum, prevents degradation with time and insulates the catalyst to changes in pH. This allows for *in situ* generation of imaging and therapeutic agents in biological systems.

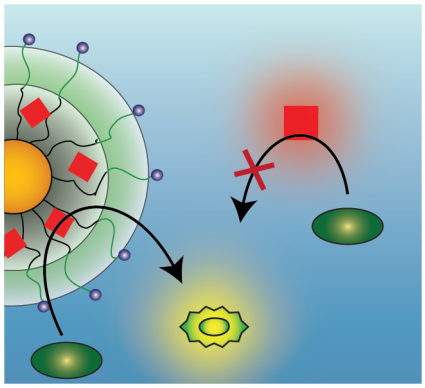

Institute and/or researcher Twitter usernames:

References

1 C. R. Bertozzi, *Acc. Chem. Res.* **2011**, *44*, 651–653.
2. J. A. Prescher, C. R. Bertozzi, *Nat. Chem. Biol.* **2005**, *1*, 13–21.
3. E. M. Sletten, C. R. Bertozzi, *Angew. Chemie - Int. Ed.* **2009**, *48*, 6974–6998.
4 R. Cao-Milan, L. D. He, S. Shorkey, G. Y. Tonga, L.-S. Wang, X. Zhang, I. Uddin, R. Das, M. Sulak, V. R. Rotello, *Mol. Syst. Des. Eng.*, **2017**,*2*, 624-628
5 J. Li, P. R. Chen, *Nat. Chem. Biol.* **2016**, *12*, 129–137.
6 J. Wu, X. Wang, Q. Wang, Z. Luo, S. Li, Y. Zhu, L. Qin, H. Wei, *Chem. Soc. Rev.* **2019**, *48*, 1004-1076.
7 Y. Huang, J. Ren, X. Qu, *Chem. Rev.* **2019,** *119,* 4357-4412
8 G. Y. Tonga, Y. Jeong, B. Duncan, T. Mizuhara, R. Mout, R. Das, S. T. Kim, Y. C. Yeh, B. Yan, S. Hou, et al., *Nat. Chem.* **2015**, *7*, 597–603.
9 F. Wang, Y. Zhang, Z. Du, J. Ren, X. Qu, *Nat. Commun.* **2018**, *9*, 1209.
10 C. Streu, E. Meggers, *Angew. Chemie Int. Ed.* **2006**, *45*, 5645–5648.
11 C. Vidal, M. Tomástomás-Gamasa, A. Gutiérrezgutiérrez-Gonzaíez, J. J. Mascareñ, *J. Am. Chem. Soc* **2019**, *141*, 5129.
12 T. Völker, E. Meggers, *Curr. Opin. Chem. Biol.* **2015**, *25*, 48–54.
13 J. M. Chalker, C. S. C. Wood, B. G. Davis, *J. Am. Chem. Soc.* **2009**, *131*, 16346–16347.
14 J. Li, J. Yu, J. Zhao, J. Wang, S. Zheng, S. Lin, L. Chen, M. Yang, S. Jia, X. Zhang, et al., *Nat. Chem.* **2014**, *6*, 352–361.
15 R. M. Yusop, A. Unciti-Broceta, E. M. V. Johansson, R. M. Sánchez-Martín, M. Bradley, *Nat. Chem.* **2011**, *3*, 239–243.
16 M. Sancho-Albero, B. Rubio-Ruiz, A. M. Pérez-López, V. Sebastián, P. Martín-Duque, M. Arruebo, J. Santamaría, A. Unciti-Broceta, *Nat. Catal.* **2019**, *2*, 864–872.
17 M. A. Miller, B. Askevold, H. Mikula, R. H. Kohler, D. Pirovich, R. Weissleder, *Nat. Commun.* **2017**, *8*, 15906.
18 P. Destito, A. Sousa-Castillo, J. R. Couceiro, F. López, M. A. Correa-Duarte, J. L. Mascareñas, *Chem. Sci.* **2019**, *10*, 2598–2603.
19 M. Martínez-Calvo, J. R. Couceiro, P. Destito, J. Rodríguez, J. Mosquera, J. L. Mascareñas, *ACS Catal.* **2018**, *8*, 6055–6061.
20 P. K. Sasmal, S. Carregal-Romero, A. A. Han, C. N. Streu, Z. Lin, K. Namikawa, S. L. Elliott, R. W. Köster, W. J. Parak, E. Meggers, *ChemBioChem* **2012**, *13*, 1116–1120.
21 M. Martínez-Calvo, J. L. Mascareñas, *Coord. Chem. Rev.* **2018**, *359*, 57–79.
22 Y. Bai, J. Chen, S. C. Zimmerman, *Chem. Soc. Rev.* **2018**, *47*, 1811–1821.
23 X. Zhang, R. Huang, S. Gopalakrishnan, R. Cao-Milán, V. M. Rotello, *Trends Chem.* **2019**, *1*, 90–98.
24 Y. Jeong, G. Y. Tonga, B. Duncan, B. Yan, R. Das, C. Sahub, V. M. Rotello, *Small* **2018**, *14*, 1702198.
25 A. Unciti-Broceta, E. M. V. Johansson, R. M. Yusop, R. M. Sánchez-Martín, M. Bradley, *Nat. Protoc.* **2012**, *7*, 1207–1218.
26 P. Destito, A. Sousa-Castillo, J. R. Couceiro, F. López, M. A. Correa-Duarte, J. L. Mascareñas, *Chem. Sci.* **2019**, *10*, 2598–2603.
27 R. Cao-milan, S. Gopalakrishnan, L. D. He, R. Huang, L. Wang, L. Castellanos, D. C. Luther, R. F. Landis, J. M. V Makabenta, C. Li, et al., *Chem* **2020**, https://doi.org/10.1016/j.chempr.2020.01.015
28 R. Das, R. F. Landis, G. Y. Tonga, R. Cao-Milán, D. C. Luther, V. M. Rotello, *ACS Nano* **2019**, *13*, 229–235.
29 A. Gupta, R. Das, G. Yesilbag Tonga, T. Mizuhara, V. M. Rotello, *ACS Nano* **2018**, *12*, 89–94.
30 C. K. Kim, P. Ghosh, C. Pagliuca, Z. Zhu, S. Menichetti, V. M. Rotello, *J. Am. Chem. Soc.* **2009**, *131*, 1360–1361.
31 K. Saha, M. Rahimi, M. Yazdani, S. T. Kim, D. F. Moyano, S. Hou, R. Das, R. Mout, F. Rezaee, M. Mahmoudi, et al., *ACS Nano* **2016**, *10*, 4421–4430.
32 X. Zhang, Y. Liu, S. Gopalakrishnan, L. Castellanos-Garcia, G. Li, M. Malassine, I. Uddin, R. Huang, D. C. Luther, R. W. Vachet, et al. *ACS Nano* **2020**, https://doi.org/10.1021/acsnano.0c00629
33 S. Brauch, M. Henze, B. Osswald, K. Naumann, L. A. Wessjohann, S. S. Van Berkel, B. Westermann, *Org. Biomol. Chem.,* **2012**, *10*, 958-965

34 J. Gooch, V. Abbate, B. Daniel, N. Frascione, *Analyst*, **2016**,*141*, 2392-2395